Published in final edited form as:

Sci Transl Med. 2014 May 21; 6(237): 237ra67. doi:10.1126/scitranslmed.3007974.

Disruption of CXCR2-Mediated MDSC Tumor Trafficking Enhances Anti-PD1 Efficacy

Steven L. Highfill, **Yongzhi Cui**, **Amber J. Giles**, **Jillian P. Smith**, **Hua Zhang**, **Elizabeth Morse**, **Rosandra N. Kaplan**, **Crystal L. Mackall***

Pediatric Oncology Branch, National Cancer Institute, National Institutes of Health, Bethesda, MD 20892, USA.

Abstract

Suppression of the host's immune system plays a major role in cancer progression. Tumor signaling of programmed death 1 (PD1) on T cells and expansion of myeloid-derived suppressor cells (MDSCs) are major mechanisms of tumor immune escape. We sought to target these pathways in rhabdomyosarcoma (RMS), the most common soft tissue sarcoma of childhood. Murine RMS showed high surface expression of PD-L1, and anti-PD1 prevented tumor growth if initiated early after tumor inoculation; however, delayed anti-PD1 had limited benefit. RMS induced robust expansion of $CXCR2^{+}CD11b^{+}Ly6G^{hi}$ MDSCs, and CXCR2 deficiency prevented $CD11b^{+}Ly6G^{hi}$ MDSC trafficking to the tumor. When tumor trafficking of MDSCs was inhibited by CXCR2 deficiency, or after anti-CXCR2 monoclonal antibody therapy, delayed anti-PD1 treatment induced significant antitumor effects. Thus, $CXCR2^{+}CD11b^{+}Ly6G^{hi}$ MDSCs mediate local immunosuppression, which limits the efficacy of checkpoint blockade in murine RMS. Human pediatric sarcomas also produce CXCR2 ligands, including CXCL8. Patients with metastatic pediatric sarcomas display elevated serum CXCR2 ligands, and elevated CXCL8 is associated with diminished survival in this population. We conclude that accumulation of MDSCs in the tumor bed limits the efficacy of checkpoint blockade in cancer. We also identify CXCR2 as a novel target for modulating tumor immune escape and present evidence that $CXCR2^{+}CD11b^{+}Ly6G^{hi}$ MDSCs are an important suppressive myeloid subset in pediatric sarcomas. These findings present a translatable strategy to improve the efficacy of checkpoint blockade by preventing trafficking of MDSCs to the tumor site.

INTRODUCTION

The programmed death 1 (PD1) receptor is a critical immune checkpoint that serves to control inflammation and self-reactivity (1–4). Signaling of PD1 on T cells via PD-L1 (B7-H1) or PD-L2 (B7-DC) inhibits T cell receptor–mediated activation by recruitment of the SHP2 phosphatase (2). Since its discovery in 1992 (5), it has become increasingly apparent that cancers often use PD1 signaling to mediate immune escape. Tumor expression of PD-

*Corresponding author. cm35c@nih.gov.

Author contributions: S.L.H. designed and performed experiments and wrote the manuscript; Y.C., A.J.G., J.P.S., H.Z., and E.M. performed experiments; R.N.K. edited the manuscript; and C.L.M. designed experiments, provided funding, and edited the manuscript.

Competing interests: The authors declare that they have no competing interests.

L1 inhibits tumor-reactive T cells in animal models (6–8), and some clinical studies show correlations between tumor expression of PD-L1 and PD-L2 and adverse outcomes (9, 10). Early evidence for a role for the PD1/PD-L1 axis in tumor immune escape comes from clinical trials of anti-PD1 and PD-L1 monoclonal antibody (mAb) therapy involving more than 500 patients with advanced cancer. Objective responses were observed in 6 to 28% of patients with melanoma, renal cell carcinoma, and non–small cell lung cancer (11, 12). Thus, although PD1 signaling on T cells is one important mechanism used by tumors to escape antitumor immune responses, interruption of this axis alone induces meaningful antitumor effects in only a minority of cases, suggesting that other mechanisms also contribute to immune evasion. Response rates for this class of therapeutics could potentially be enhanced if other mechanisms of immune escape are simultaneously targeted.

Myeloid-derived suppressor cells (MDSCs) expand in tumor-bearing hosts and contribute to tumor immune evasion through a variety of mechanisms, including oxidative stress and nutrient depletion via inducible nitric oxide synthase (iNOS) and arginase production (13). MDSCs are immature myeloid cells that can be phenotypically divided into monocytic (MoMDSCs) ($CD11b^{+}Ly6C^{hi}$) and granulocytic (GrMDSCs) ($CD11b^{+}Ly6G^{hi}$) subsets. MoMDSCs have been demonstrated to expand in response to granulocyte-macrophage colony-stimulating factor (GM-CSF) in mice bearing B16F10 melanoma, and to express the CCR2 chemokine receptor (14). Although CCR2 is not required for the suppressive activity of MoMDSCs, previous work demonstrated that depletion of $CCR2^{+}$ MoMDSCs enhances the efficacy of adoptive T cell therapy.

Here, we report that murine rhabdomyosarcoma (RMS) primarily induces the expansion of granulocytic $CXCR2^{+}CD11b^{+}Ly6G^{hi}$ MDSCs, and demonstrate that CXCR2 is required for trafficking of these MDSCs to the tumor bed. We find that MDSC-mediated suppression of antitumor immunity is a local phenomena limited to the tumor bed because inhibition of MDSC trafficking to the tumor enhances the potency of PD1 checkpoint blockade. This work identifies CXCR2 as a new target for therapies aimed at inhibiting MDSC recruitment, and provides a rationale for combining immune checkpoint inhibitors with agents designed to prevent MDSC-mediated immune suppression for cancer therapy.

RESULTS

The effectiveness of PD1 blockade in RMS is diminished in the presence of established tumor

We tested PD1 blockade therapy in embryonal RMS using M3-9-M, a cell line derived from a spontaneous RMS occurring in a male $p53^{+/-} \times HGF^{+/-}$ transgenic mouse (15). M3-9-M grows rapidly after orthotopic inoculation of 1×10^{6} cells into the gastrocnemius of female mice, leading to 100% mortality by day 25 (Fig. 1A). Progressive tumor growth occurred despite activation of peripheral T cells, as evidenced by increased PD1 and Tim-3 expression on circulating T cells by day 20 (Fig. 1B and fig. S12). M3-9-M constitutively expressed PD-L1 (Fig. 1C, left panel), leading us to postulate that tumor-induced PD1 signaling on T cells contributes to immune escape in M3-9-M RMS. To test this, we administered blocking anti-PD1 mAbs beginning on the day of tumor inoculation. Female mice treated in this manner had 100% survival with no evidence of tumor development (Fig. 1A), thus

implicating PD1 in immune escape by murine RMS. To test whether anti-PD1 mAbs could induce regression of an established M3-9-M tumor, anti-PD1 treatment was delayed until day 7, at which time the mean tumor size was about 90 mm^2 (Fig. 1D). Delayed anti-PD1 modestly decreased the tumor growth rate and mediated a minor, albeit statistically significant, improvement in survival (Fig. 1D, right panel). Although delayed treatment did not lead to tumor regression, M3-9-M-bearing mice treated with delayed anti-PD1 demonstrated significantly more interferon-γ–positive (IFN-γ^+) and tumor necrosis factor–α–positive (TNF-α^+) $CD8^+$ T cells in the spleen (Fig. 1E) and tumor (Fig. 1F and fig. S13) than untreated control mice, suggesting that delayed anti-PD1 treatment induced immune activation that was insufficient to mediate tumor regression. The antitumor effects observed were absolutely dependent on host T cells because administration of anti-PD1 to $RAG^{-/-}$ mice lacking T cells resulted in no difference in tumor growth (fig. S1). We also tested the therapeutic efficacy of anti-PD1 in animals inoculated with 76–9, another embryonal RMS tumor (16) expressing PD-L1 (Fig. 1C, right panel). The effects were less potent than those observed with M3-9-M, but PD1 blockade initiated at the time of tumor inoculation did result in significant antitumor effects (Fig. 1G), whereas delayed treatment beginning on day 7 had no significant impact on tumor growth (Fig. 1H).

M3-9-M expresses HY, the male minor histocompatibility antigen complex (Fig. 2A), and we found that a substantial component of the antitumor effects observed was due to the capacity for PD1 blockade to augment immunity toward HY-associated antigens. This was evidenced by the fact that PD1 blockade was more effective in female rather than in male M3-9-M-bearing animals treated with the same regimen (Fig. 2, B and C). In addition, splenic T cells taken from M3-9-M tumor–bearing mice demonstrated low levels of immune reactivity to immunodominant class I– and class II–restricted HY antigens, which was substantially increased after treatment with anti-PD1 (Fig. 2D). This effect is not due to a nonspecific enhancement of T cell responsiveness in anti-PD1–treated mice because tumor-free mice and mice bearing 76–9 tumors, which do not express HY, did not show significant increases in HY-specific IFN-γ production after anti-PD1 therapy (Fig. 2D), nor did M3-9-M-bearing mice develop measurable immune responses to E7 or *Trypanosoma cruzi*, class I– and class II–binding control peptides, respectively. Together, these data identify PD1 signaling in T cells as one mechanism used by RMS to evade immune responses, and illustrate that the efficacy of anti-PD1 treatment is significantly reduced with increasing tumor burden, raising the prospect that other mechanisms of immune escape contribute to tumor growth in this model. Furthermore, PD1 blockade is more effective in immunogenic tumors, such as those expressing a minor histocompatibility antigen, than in settings where tumor antigens induce less potent immune responses.

RMS tumor progression is associated with preferential expansion of $CD11b^+Ly6G^{hi}$ MDSCs

To explore potential alternative mechanisms through which RMS may evade host immunity, we investigated whether RMS promotes expansion of MDSCs that limit the efficacy of immune-based therapy. MDSCs were increased in the peripheral blood as early as day 10 after inoculation of RMS into mice. By day 20, MDSCs represented a sizable fraction of the spleen and tumor (Fig. 3, A and B). Further characterization of MDSC subsets revealed a

surface expression pattern and morphology consistent with previously published observations, in that GrMDSCs were CD11b^{+}Ly6C^{lo}Ly6G^{+}CD115^{-}F4/80^{-} with ring-shaped morphology and MoMDSCs had the phenotype CD11b^{+}Ly6C^{hi}Ly6G^{-}CD115^{+}F4/80^{+} with mononuclear morphology (figs. S2A and S3) (17).

To determine which tumor-derived cytokines were responsible for MDSC expansion, we analyzed M3-9-M cell culture supernatants for known MDSC-inducing cytokines. G-CSF, GM-CSF, VEGF (vascular endothelial growth factor), TGFβ1 (transforming growth factor–β1), and SCF (stem cell factor) concentrations were all significantly increased in M3-9-M supernatant compared with control samples (fig. S2B). Furthermore, animals treated with anti–G-CSF neutralizing antibodies demonstrated less MDSC expansion (fig. S2C). Thus, murine RMS produces a variety of cytokines previously implicated in MDSC expansion, and G-CSF directly contributes to MDSC expansion in this model.

To confirm that the CD11b^{+}Ly6G^{hi} and CD11b^{+}Ly6C^{hi} subsets expanded in RMS-bearing hosts were suppressor cells, we electronically sorted CD11b^{+}Ly6G^{hi} and CD11b^{+}Ly6C^{hi} cells from tumor-bearing animals and assessed their capacity to produce arginase-1 and iNOS, mediators of MDSC immune suppression. As shown in Fig. 3C, CD11b^{+}Ly6G^{hi} and CD11b^{+}Ly6C^{hi} cells from tumor-bearing mice express arginase-1 and iNOS, whereas these genes are not expressed by cells bearing the same phenotype in the bone marrow (BM) of non–tumor-bearing mice. Notably, higher levels of arginase-1 were found in the CD11b^{+}Ly6G^{hi} subset, whereas higher levels of iNOS were observed in the CD11b^{+}Ly6C^{hi} subset (Fig. 3D). Rodriguez *et al.* (18) previously showed a direct correlation between L-arginine depletion and decreased expression of CD3ζ on peripheral T cells. When we analyzed the expression of CD3ζ in CD4^{+} and CD8^{+} peripheral blood T cells of tumor-free compared with tumor-bearing mice, we observed a significant decrease in the MFI (Fig. 3E), consistent with a model wherein RMS tumor–bearing mice experience T cell dysfunction due, in part, to MDSC-mediated depletion of L-arginine. We next sorted the CD11b^{+}Ly6G^{hi} and CD11b^{+}Ly6C^{hi} subsets from the spleens of M3-9-M tumor–bearing mice and evaluated their capacity to suppress proliferation of anti-CD3/anti-CD28–activated splenic T cells. At MDSC/T cell ratios of 1:2, Ly6G^{hi} MDSCs inhibited T cell proliferation by about 90% and remained highly suppressive even at MDSC/T cell ratios of 1:8. Although Ly6C^{hi} MDSCs also suppressed T cell proliferation, they were less potent than Ly6G^{hi} MDSCs and their suppressive potential was more readily diminished with decreasing MDSC/T cell ratios (Fig. 3F). We next sought to determine whether T cell suppression mediated by CD11b^{+}Ly6G^{hi} cells was reversible upon inhibition of arginase-1 and/or iNOS. To do this, we sorted CD11b^{+}Ly6G^{hi} cells from the tumors of M3-9-M-bearing animals and measured inhibition of T cell proliferation after addition of nor-NOHA (N^{w}-hydroxy-nor-arginine) (arginase inhibitor) or L-NMMA (L-N^{G}-monomethyl-arginine-citrate) (iNOS inhibitor). Both inhibitors significantly reduced CD4^{+} and CD8^{+} T cell suppression, though inhibition of arginase-1 (nor-NOHA) led to a larger decrease in suppressive potential (Fig. 3G), and we did not observe additive effects, suggesting that the effect of iNOS in this model system may be predominantly due to depletion of L-arginine. Both peripheral blood CD11b^{+}Ly6G^{hi} and CD11b^{+}Ly6C^{hi} cells expressed PD-L1 (Fig. 3H), but not PD-L2 (fig. S3B). Regulatory T cells, CD4^{+}CD25^{+}FoxP3^{+}, were also monitored during tumor progression, and we observed

no increase in T regulatory (T_{reg}) frequency in the blood of tumor-bearing mice in this model (fig. S4).

CD11b^{+}Ly6G^{hi} MDSCs require CXCR2 to traffic to RMSs

We next searched for mechanisms through which MDSCs traffic to the RMS tumor bed, where presumably they mediate their most potent immunosuppressive effect. The minor CD11b^{+}Ly6C^{hi} fraction expressed the chemokine receptor CCR2 as previously reported (Fig. 4A) (14), whereas the major circulating CD11b^{+}Ly6G^{hi} fraction expressed the chemokine receptor CXCR2 and did not express CCR2. We tested whether RMS tumors produce and secrete ligands for CXCR2 and found that both M3-9-M and 76–9 RMS expressed message for CXCL1 and CXCL2 (Fig. 4B), and culture supernatant taken from both cell lines contained high concentrations of CXCL1 protein, whereas M3-9-M also produced high concentrations of CXCL2 protein (Fig. 4C). Note that supernatants taken from two nonsarcoma tumor cell lines, B16 and EL4, did not contain either CXCL1 or CXCL2, suggesting that chemokine production may be linked with tumor histotype. CXCR2 can also bind CXCL5 and CXCL7; however, protein levels of these ligands in cell culture supernatants taken from M3-9-M and 76–9 cultures were below the limit of detection (19 pg/ml, fig. S5).

We next investigated whether the RMS production of CXCR2 ligands induced a chemokine gradient in vivo. We focused on the M3-9-M model because of its high vascularity and ease of obtaining blood samples directly from the tumor. Indeed, blood obtained from within the tumors of M3-9-M-bearing mice had significantly higher levels of CXCL1 and CXCL2 protein than that taken from the retro-orbital sinus of the same mice (Fig. 4D), providing direct evidence for a chemokine gradient in vivo that could mediate efficient trafficking of CXCR2^{+} MDSCs to the tumor bed. We next used an in vitro migration assay in which M3-9-M tumor cells were plated in the bottom chamber, and sorted CD11b^{+}Ly6G^{hi} cells isolated from the blood of tumor-bearing animals were added to the top chamber of a 96-well Transwell, with or without blocking antibodies for CXCR2, CXCL1, or CXCL2. After 8 hours, migration of CD11b^{+}Ly6G^{hi} cells was enhanced in the presence of M3-9-M tumor ($P < 0.001$) (Fig. 4E). Blocking antibodies for CXCL1 and CXCL2 significantly inhibited migration ($P = 0.007$ and $P = 0.003$, respectively) when used alone, and their effects were additive ($P < 0.001$). Inhibiting the receptor on MDSCs using an anti-CXCR2 blocking antibody was equivalent to blocking CXCL1 and CXCL2 ($P < 0.001$), demonstrating that other CXCR2 ligands were not mediating this effect (Fig. 4E). Similar results were observed when we used CD11b^{+}Ly6G^{hi} isolated from the spleen of tumor-bearing mice (fig. S6).

We next tested whether CD11b^{+}Ly6G^{hi} migration to RMS in vivo is dependent on CXCR2. Because of the fact that CXCR2$^{-/-}$ mice are poor breeders and because we wanted to study the effects of isolated loss of CXCR2 in the hematopoietic compartment, we generated CXCR2$^{-/-}$ > wild-type and control wild-type > wild-type BM radiation chimeras. After hematopoietic reconstitution, mice were inoculated with RMS cells, and then CD11b^{+}Ly6G^{hi} cells within the tumor were quantified. Compared to recipients of wild-type BM, we observed a significant decrease in the percentage and absolute numbers of CD11b^{+}Ly6G^{hi} cells within M3-9-M and 76–9 tumors in mice with a CXCR2$^{-/-}$ hematopoietic

compartment (Fig. 5, A to C). Immunofluorescent staining confirmed reduced numbers of total $CD11b^+$ cells, $Ly6G^+$ cells, and $CD11b^+Ly6G^+$ cells in recipients of $CXCR2^{-/-}$ marrow (Fig. 5E). The spleens of M3-9-M– bearing (fig. S7, A, B, and D) or 76–9-bearing (fig. S7C) animals with $CXCR2^{-/-}$ marrow showed significant increases in percentage and absolute numbers of $CD11b^+Ly6G^{hi}$ cells compared to wild-type mice with the same tumors, presumably as a result of diminishing trafficking into other tissues. Thus, CXCR2-mediated signals are essential for MDSC trafficking into the tumor but are not required for egress from the BM, because significantly more $CXCR2^{-/-}$ MDSCs are present in the peripheral blood (fig. S7E) and spleens of tumor-bearing mice.

We observed a modest decrease in M3-9-M and 76–9 tumor growth rate in recipients of $CXCR2^{-/-}$ marrow compared to recipients of wild-type marrow (Fig. 5D). Because diminished MDSC migration into the tumor bed could diminish tumor growth rates through effects on tumor angiogenesis, we evaluated CD31 expression in tumors from mice with $CXCR2^{-/-}$ via immunofluorescence. We did not observe significant reductions in angiogenesis between tumors with $CXCR2^{-/-}$ MDSCs compared with controls, which led us to conclude that the diminished tumor growth observed was not primarily due to antiangiogenic effects (fig. S7F). Together, these results demonstrate that murine RMS tumors are dependent on interactions between CXCR2 and CXCR2 ligands to at tract suppressive MDSCs to the tumor microenvironment, and are consistent with a model wherein immune-mediated suppression via MDSCs modestly contributes to tumor growth.

Patients with metastatic sarcomas show elevated levels of CXCR2 ligands, and CXCL8 elevation is associated with adverse prognostic significance in metastatic pediatric sarcomas

The data presented thus far reveal a critical role for CXCR2 signaling in recruiting $CD11b^+Ly6G^{hi}$ MDSCs to murine RMS. We next sought to explore whether human pediatric sarcomas use the same axis. In humans, CXCL1 and CXCL8 are the major ligands for CXCR2 (19). We tested supernatants taken from four pediatric sarcoma cell lines for CXCL1 and CXCL8: All produced significant amounts of CXCL8 and two produced high levels of CXCL1 (Fig. 6A). We next measured levels of CXCR2 ligands in serum from children and young adults with metastatic pediatric sarcomas obtained at the time of enrollment on immunotherapy trials ($n = 53$) compared with healthy donors ($n = 22$). As shown in Fig. 6B, patients with pediatric sarcomas had significant elevations in both CXCL8 and CXCL1 compared to healthy donors (CXCL8, $P = 0.001$; CXCL1, $P = 0.04$). Sarcoma-specific evaluation confirmed significantly elevated CXCL8 levels in RMS ($P = 0.02$, $n = 14$), desmoplastic small round cell tumor ($P = 0.002$, $n = 8$), and osteosarcoma ($P = 0.04$, $n = 6$), and significant differences in CXCL1 levels were observed for Ewing sarcoma ($P = 0.04$), RMS ($P = 0.03$), and desmoplastic small round cell tumor ($P = 0.005$) (fig. S8). To explore whether supranormal CXCL8 levels correlated with diminished overall survival in this population, an actuarial analysis was performed. With a median potential follow-up of 37.6 months, median survival for patients with elevated versus normal CXCL8 levels was 12.3 months versus 47.2 months [hazard ratio, 2.29; 95% confidence interval (CI), 1.12 to 4.69; $P = 0.024$]. As shown in Fig. 6C, mean CXCL8 levels in patients who are currently alive was 80.5 pg/ml compared to a mean CXCL8 level of 222.8 pg/ml in patients who have

died ($P = 0.005$). Similar prognostic differences were not observed for CXCL1 levels because the hazard ratio for patients with elevated CXCL1 levels was 1.55 (95% CI, 0.72 to 3.31; $P = 0.26$). These results demonstrate that the chemokine axis identified as essential for MDSC recruitment in murine RMS is also active in patients with pediatric sarcomas, and are consistent with a model where CXCR2 ligands contribute to poor clinical outcomes.

Prevention of MDSC trafficking to the tumor microenvironment enhances immune checkpoint blockade efficacy

Given the capacity for MDSCs to limit antitumor T cell responses, we sought to test whether anti-PD1 therapy was more effective when $CD11b^{+}Ly6G^{hi}$ MDSCs were prohibited from trafficking to the tumor microenvironment. Mice reconstituted with a wild-type or $CXCR2^{-/-}$ hematopoietic compartment were inoculated with M3-9-M RMS cells on day 0, and anti-PD1 treatment was begun on day 12, when the tumor was well established. PD1 blockade in hosts reconstituted with wild-type hematopoietic cells was ineffective (Fig. 7A, left). In contrast, mice reconstituted with $CXCR2^{-/-}$ hematopoietic cells and then treated with anti-PD1 experienced significant reductions in tumor growth (Fig. 7A, middle). Kaplan-Meier survival analysis in M3-9-M–bearing mice shows a modest but significant difference in median survival between wild type and wild type + anti-PD1 (median survival of 42.5 days versus 53 days, respectively), whereas mice with $CXCR2^{-/-}$ marrow experienced a much larger increase in median survival after anti-PD1 therapy ($P < 0.001$; median survival of 57 days versus undefined) (Fig. 7A, right). This experiment was mirrored by results using the 76–9 RMS tumor model, where tumors are less immunogenic because of the absence of the minor histocompatibility antigen HY. Here, hosts with wild-type marrow were afforded no significant survival benefit from anti-PD1 therapy ($P = 0.06$, median survival of 42 days versus 44 days), whereas hosts with $CXCR2^{-/-}$ marrow displayed significant improvements in overall survival ($P = 0.009$, median survival of 38 days versus 60 days) (Fig. 7B).

Consistent with our results demonstrating that anti-PD1 mediates its effects in this model by augmenting T cell–mediated antitumor immunity, we observed increases in tumor-infiltrating $CD8^{+}$ T cells after anti-PD1 therapy (Fig. 7C, left). $CXCR2^{-/-}$ hosts had significantly diminished MDSCs within the tumor (Fig. 7C, middle), which resulted in a significant increase in the ratio of T cell/MDSC in these hosts when given anti-PD1 therapy (Fig. 7C, right). In accordance with this, we observed a significant increase in the number of activated $CD8^{+}$ T cells within the tumor of $CXCR2^{-/-}$ mice when compared to wild-type mice (Fig. 7D), which resulted in an increased IFN-g concentration within the serum of $CXCR2^{-/-}$ mice that were treated with anti-PD1 (Fig. 7E). No difference in PD-L1 expression was observed on RMS-expanded GrMDSCs or MoMDSCs from wild-type B6 mice versus $CXCR2^{-/-}$ mice (fig. S9). We conclude that the diminished numbers of suppressive $CXCR2^{+}CD11b^{+}Ly6G^{hi}$ cells within the tumor microenvironment significantly enhance the antitumor effects of anti-PD1 immune therapy. This occurs despite systemic expansion and accumulation of immunosuppressive $CXCR2^{+}CD11b^{+}Ly6G^{hi}$ MDSCs within the spleen and other tissues of treated mice and results from improved functionality of tumor-infiltrating T cells when $CXCR2^{+}CD11b^{+}Ly6G^{hi}$ cells are absent from the tumor bed.

We next sought to test whether targeting MDSCs with anti-CXCR2 mAbs, an approach that would be potentially clinically applicable, would yield similar antitumor effects. We inoculated mice with M3-9-M RMS tumor cells on day 0 and then administered anti-CXCR2 mAbs on days 6 and 10. FACS analysis of peripheral blood (Fig. 8, A and B) and tumor digests (Fig. 8D) on day 15 demonstrated that anti-CXCR2 induced significant reductions in $CD11b^{+}Ly6G^{hi}$ cells when compared to nontreated controls. We observed no significant change in the frequency or number of $Ly6G^{hi}$ MDSCs in the spleen after anti-CXCR2 therapy (Fig. 8C). We conclude that anti-CXCR2 likely diminishes tumor bed–associated GrMDSCs by modulating tumor trafficking rather than by inducing depletion.

Tumor growth curves and survival analysis show that combination therapy using anti-CXCR2 plus anti-PD1 therapy leads to greater benefit compared to either agent alone (Fig. 8E). We also evaluated the efficacy of antibody treatment in the less immunogenic 76–9 RMS model lacking HY reactivity. Similarly, the dual therapeutic intervention reduced $CD11b^{+}Ly6G^{hi}$ cells in the peripheral blood and delayed tumor growth, leading to significant increases in overall survival (fig. S10, A and B). Together, these data implicate tumor-induced MDSCs in preventing the full benefit of immune checkpoint blockade and offer a translatable, therapeutic option to improve the efficacy of checkpoint blockade by targeting the $CXCR2^{+}$ subset of MDSCs.

DISCUSSION

Immunotherapy for cancer has had an increasing trajectory of success, and checkpoint blockade is among the most successful immunotherapeutic strategies developed thus far. Checkpoint inhibitors comprise a class of agents that disrupt inhibitory signals delivered to T cells. Antibodies that block CTLA4 signaling prolong survival in patients with metastatic malignant melanoma (20, 21), and antibodies that block PD1 signaling or PD-L1 binding to PD1 mediate objective antitumor responses in patients with melanoma, non–small cell lung cancer, and renal cell carcinoma (11, 12). Combination regimens appear to be even more potent with response rates of 53% in metastatic melanoma (22). Despite this progress, the percentage of cancer patients who benefit from checkpoint inhibitors administered as single agents is small, with <30% of patients treated with each of these agents experiencing a clinical response, and it remains unknown whether the combination regimen will be equally potent in nonmelanoma histologies. The murine model of RMS presented here illustrates the limitations of checkpoint blockade as a single treatment modality. Tumor development is completely inhibited when animals are treated with anti-PD1 at the time of tumor inoculation, but anti-PD1 has only weak effects on established tumors, regardless of whether they are immunogenic, as is the case with M3-9-M, which expresses a minor histocompatibility antigen. Thus, factors beyond PD1 signaling contribute to tumor immune escape in vivo.

Expansion of MDSCs is a major mechanism used by cancers to escape immune surveillance. In mice bearing RMS, we observed significant increases in the frequency of total MDSCs in peripheral blood as early as 10 days after tumor injection, before the development of measurable tumors. By day 20 after RMS inoculation, MDSCs accounted for up to 80% of total cells in the blood, 11% of total cells in the spleen, and 25% of total cells in the tumor.

MoMDSCs and GrMDSCs have been observed in tumor-bearing mice and in humans with cancer, with varying frequencies depending on the tumor histotype (17, 23–25). GrMDSCs ($CD11b^{+}Ly6G^{hi}$) were preferentially expanded in all three compartments analyzed in this model, and, on a per cell basis, GrMDSCs proved to be the more suppressive MDSC subtype. Indeed, although numerous reports describe the MoMDSCs as the more suppressive subtype (25–27), several previous models involving murine melanoma, lung carcinoma, and lymphoma models observed that GrMDSCs are more suppressive (28). In our model, suppressive capacity is likely mediated to a large extent via L-arginine depletion because inhibitors of enzymes that use L-arginine as a substrate including arginase-1 (nor-NOHA) and iNOS (L-NMMA) significantly reversed the T cell suppression. Moreover, arginase-1 levels were about fourfold higher in GrMDSCs versus MoMDSCs in RMS-bearing animals.

The distinction between $CD11b^{+}Ly6G^{hi}$ and $CD11b^{+}Ly6C^{hi}$ MDSCs and the fact that $CD11b^{+}Ly6G^{hi}$ MDSCs are the predominant mediator of immune escape is an essential observation in this model system, because previous reports emphasized a critical role for $CCR2^{+}$ ligands in tumor trafficking of MoMDSCs (14). Note that in our model system, the relative frequency of MoMDSCs compared to GrMDSCs is reduced in the blood compared to the spleen (1:11 blood versus 1:5 spleen), and the relative frequency is the lowest in the tumor (1:113). Thus, it is possible that MoMDSCs preferentially traffic from blood to the spleen rather than to the tumor. One plausible explanation for the altered migratory patterns of MoMDSCs comes from a study by Molon et al. (29), which showed that CCL2 undergoes posttranslational modification (nitration) within the tumor bed, which makes it less effective in attracting $CCR2^{+}$ cells. In contrast, $CD11b^{+}Ly6G^{hi}$ cells, the predominant MDSC subtype present in this model system, do not express CCR2. Rather, $CD11b^{+}Ly6G^{hi}$ cells expanded by murine RMS express CXCR2 and trafficked to tumor as a result of tumor production of CXCR2 ligands.

Comparison of CXCR ligands driving MDSC accumulation across species is complex because there are significant differences in this family of molecules between mice and humans. In humans, CXCL8 and CXCL6 signal through both CXCR1 and CXCR2, whereas the other CXC chemokine ligands (CXCL1, CXCL2, CXCL3, CXCL5, and CXCL7) signal only via CXCR2 (30). Hence, in humans, CXCR1 and CXCR2 likely both play a role in modulating granulocyte trafficking. In Fig. 4E, we show a significant decrease in the number of MDSCs that migrate toward tumor attractant when we use anti-CXCL1 and anti-CXCL2 blockade. The fact that migration is not completely inhibited when CXCR2 is absent raises the possibility that other chemokines or soluble factors may also be involved in migration of these cells. We examined tumor cell supernatant for all four CXCR2 ligands and discovered that CXCL5 and CXCL7 were not produced by the tumor cell lines (fig. S5). Also, mice lack a CXCL8 homolog, and the functionality of the murine CXCR1 chemokine receptor is not well characterized. One manuscript indicated that mCXCR1 predominantly engaged mouse CXCL6 (31). However, in our model system, in vivo trafficking of GrMDSCs was essentially entirely inhibited in mice lacking CXCR2. Therefore, CXCR2 appears to be the dominant CXC chemokine receptor on myeloid cells in mice. Chemokines that signal via CXCR2 have been shown to play a role in GrMDSC recruitment in other model systems. In murine hepatocellular carcinoma, a direct correlation between increases in hepatic CXCL1

and MDSC frequency was observed (32), and splenic MDSC accumulation was significantly reduced with anti-CXCL1 therapy. Yang *et al.* (33) showed that $Gr1^+CD11b^+$ MDSCs are recruited into murine mammary carcinomas via a CXCR2-dependent mechanism and, once there, act to promote tumor invasion and metastasis. In accordance with our data, Katoh et al. (34) recently showed that deletion of CXCR2 in a mouse model of colitis-associated tumorigenesis reduced the number of GrMDSCs within the tumor, which had a marked effect on T cell function. Finally, serum samples from patients with head and neck squamous cell carcinoma showed a strong positive correlation between GrMDSC levels and CXCL8 concentration, which was presumably tumor-derived (35). Thus, although $CD11b^+Ly6G^{hi}$ and $CD11b^+Ly6C^{hi}$ mediate immune suppression in tumor-bearing hosts via similar mechanisms with varying potencies depending on the model system studied, distinct chemokine axes regulate trafficking of these two subsets to the tumor bed.

We investigated the biologic ramifications of preventing tumor trafficking of $CD11b^+Ly6G^{hi}$ MDSCs to the RMS tumor bed. Inhibition of tumor trafficking resulted in a compensatory accumulation of $CD11b^+Ly6G^{hi}$ cells within the spleen and bloodstream of RMS-bearing hosts. These results are consistent with previous reports demonstrating that GrMDSCs at the tumor site are highly dependent on migration from the BM or spleen and undergo minimal proliferation within the tumor bed (13). Remarkably, combining checkpoint blockade with inhibition of CXCR2-mediated trafficking of BM-derived cells significantly enhanced antitumor effects, despite systemic accumulation of these cells, because we observed tumor regression in six of six mice receiving dual antibody treatment (Fig. 8C). We conclude therefore that although MDSCs can mediate systemic immunosuppression (36), local immunosuppression appears to be the major limiting factor in the response to anti-PD1 therapy in this model system. Despite impressive early effects, tumor recurrence eventually occurred in nearly all animals. The basis for late tumor immune escape in this model is currently under study but could be related to T cell exhaustion, rebound of MDSC populations after discontinuation of antibody therapy in the mAb-treated hosts, or other mechanisms. Nonetheless, these results illustrate an essential role for local immunosuppression by MDSCs in mediating tumor immune escape and highlight the potential value of therapeutics that seek to disrupt tumor trafficking of these subsets.

Clinical relevance of these findings is provided by studies in children and young adults with RMS and other embryonal sarcomas. We demonstrate that human sarcoma cell lines express CXCR2 ligands and that patients with metastatic pediatric sarcomas have elevated serum levels of CXCL1 and CXCL8. The elevations in CXCL8 were higher than that for CXCL1, consistent with a substantial literature implicating CXCL8 in various aspects of tumor growth (37). CXCL8 is induced by several oncogenes including RET, Ras (38, 39), and EGFR (40) and has been implicated in tumor survival, angiogenesis, and epithelial-mesenchymal transition (41). Similar to results reported for breast cancer (42), we observed diminished survival in pediatric sarcoma patients with elevated CXCL8 levels. It is of interest to note that the CXCL8 levels measured in patients with metastatic pediatric cancers were about one log higher than those measured in the serum of women with metastatic breast cancer (42). In a separate study investigating cryo-preserved mononuclear fractions harvested from patients with pediatric sarcoma, we observed expansion of MDSCs that express CXCR1 [interleukin-8 receptor α (IL8Rα)] (43). Although present in mononuclear

fractions, these cells show some features of polymorphonuclear differentiation including expression of $CD11b^+HLA\text{-}DR^+CD34^+CD124^+$, raising the possibility that the CXCR1/CXCR2 axis in humans may involve both polymorphonuclear and mononuclear cells. Furthermore, fresh peripheral blood, harvested from a small sampling of patients with pediatric sarcoma that was not fractionated for the mononuclear subset, demonstrated increased frequencies of circulating polymorphonuclear CXCR2-expressing cells compared to healthy donors (fig. S11). Further studies are needed to more fully assess the suppressive potential of these populations, and are under way.

The potential for clinical application of these findings is notable because there are currently no clinically applicable approaches to mitigate MDSC-mediated immune escape. The monoclonal anti-Gr1 antibody (clone RB6–8C5) effectively depletes MDSCs in tumor-bearing mice and enhances antitumor reactivity (44, 45), but human cells do not express a marker homologous to mouse Gr1, and widespread depletion of myeloid subsets would be expected to induce profound immunosuppression. All-trans retinoic acid (ATRA) appears capable of differentiating immature, suppressive MoMDSCs into mature, nonsuppressive dendritic cells, macrophages, and granulocytes, but this may also target cells other than MDSCs (such as T cells) and may potentially cause MDSC-independent effects (17, 46). Others have sought to modulate the suppressive capabilities of MDSCs using pharmacological inhibitors such as L-NMMA (a specific iNOS inhibitor), which led to a reversal of T cell dysfunction; however L-NMMA is toxic in humans and associated with myocardial depression and significantly increased mortality (47, 48). Multiple small-molecule CXCR2 inhibitors are currently under development and in clinical trials for chronic obstructive pulmonary disease. The results presented here suggest that CXCR2 inhibitors may hold promise for modulating MDSC-mediated tumor immunosuppression in settings where $CXCR2^+$ MDSCs predominate.

In summary, this report is the first to demonstrate the value of combining approaches to modulate MDSC trafficking with checkpoint blockade to treat cancer and provide clear evidence that the CXCR2 signaling is central to tumor trafficking of granulocyte MDSCs. We demonstrate that local effects of MDSCs predominate over systemic effects, because therapies that disrupt migration but lead to secondary accumulation of MDSCs potentiate immune checkpoint blockade. Finally, this model system is clinically relevant because pediatric sarcomas also produce CXCR2 ligands, patients with sarcoma have elevated levels of these ligands, and increased CXCL8 levels are associated with a poor prognosis in this high-risk population.

Limitations of the work include the limited information available regarding whether MDSCs within the tumor bed of human cancers predominantly express CXCR1 or CXCR2 and whether the associations between high circulating levels of CXCL8 and clinical outcomes relate to immunomodulatory effects or other effects mediated by CXCL8. Nonetheless, the findings presented here raise the prospect that clinical studies of agents that can block CXCR2 signaling may be beneficial either as single agents or in combination with checkpoint blockade.

MATERIALS AND METHODS

Study design

Results presented were observational studies designed to evaluate the differences among experimental treatment groups. An a priori power analysis was performed with a two-tailed, two-sample *t* test with an α of 0.05 and a power of 0.8 to detect differences between group means of twice the observed SD. All groups were randomized, and primary endpoints were survival and tumor size. All mice were humanely euthanized when tumor size reached 20 mm in any direction.

Mice and tumor lines

In animal studies, C57BL/6 (B6) and B6.129S2(C)-Cxcr2^{tm1Mwm}/j mice were purchased from the National Cancer Institute (NCI) or The Jackson Laboratory. Mice were maintained in specific pathogen–free microisolator cages in the NCI animal facility. All studies were conducted according to NCI Animal Care and Use Committee–approved protocols. Chimeric mice were generated by delivering 1000 cGy via a cesium irradiator on day 0 and transplanting 5×10^6 wild-type or CXCR2$^{-/-}$ BM cells on day 1. A hematopoietic reconstitution period of at least 30 days occurred before use in the described experiments. Mice were maintained on amoxicillin trihydrate (Clavamox) for the duration of the experiments. The M3-9-M and 76–9 cell lines were generated as previously described (15, 16). For tumor inoculation, cells were prepared as single-cell suspensions after trypsin digestion and injected into the gastrocnemius muscle in 0.2 ml of phosphate-buffered saline (PBS) using a sterile 27.5-gauge needle.

Antibodies/flow cytometry

Ly6C (clone HK1.4), anti-CD4 (clone RM4–5), anti-CD25 (clone ebio7D4), and anti–PD-L1 (clone MIH5) antibodies were purchased from eBioscience Inc.; anti-CD8a (clone 53–6.7), anti-Ly6G (clone 1A8), anti-FoxP3 (clone FJK-16a), and anti-CD11b (clone M1/70) were purchased from BD Pharmingen; anti-CXCR2 (clone TG11/CXCR2) was purchased from BioLegend. All antibodies were used following the manufacturer's recommended protocols. For CD3z, cells were permeabilized using digitonin (500 ng/ml) before adding anti-CD3ζ– phycoerythrin. Intracellular cytokine staining was performed after a 5-hour incubation of whole splenocytes with soluble anti-CD3/CD28 and monensin at 37°C and 5% CO_2. Flow cytometry was performed with FACS Fortessa or FACSAria with FACSDiva software (BD Biosciences) and analyzed by FlowJo 9 software (Tree Star). In all flow cytometry assays, background versus positive staining was ascertained using isotype controls and fluorescence minus one (FMO) controls. Circled or boxed populations quantified were identified as positive in relation to isotype and/or FMO controls. Anti-PD1 (BioXCell RMP1–14) blocking antibodies were diluted in 0.2 ml of PBS and then given intraperitoneally at 200 μg per injection on the indicated days. Anti-mouse CXCR2 (R&D Systems, MAB2164) was used at a dose of 200 μg per mouse and administered intraperitoneally on days 6 and 10 in PBS.

ELISpot assay

Our murine IFN-γ ELISpot kits (R&D Systems) were used according to the manufacturer's suggested protocol. Freshly isolated splenocytes from naïve or tumor-bearing mice treated or untreated with anti-PD1 were resuspended in HL-1 serum-free medium (BioWhittaker) supplemented with 1% penicillin/streptomycin/L-glutamine, and were plated at 10^6 per well in triplicate. Splenocytes were restimulated with the following synthetic HY-specific peptides: (i) *Uty*: the immunodominant Db–restricted HY-derived peptide corresponding to amino acids 245 to 253 (WMHHNMDLI) of the *Uty* gene product; (ii) *Dby*: the immunodominant I-Ab–restricted (NAGFNSNRANSSRSS) HY-derived peptide; and as specific controls (iii) for Db binding: the *E7* peptide (RAHYNIVTF) derived from HPV and (4) I-Ab peptide: the *T. cruzi* peptide (SHNFTLVASVIIEEA). After wash steps and incubation with a biotinylated IFN-γ detection antibody, alkaline-phosphatase conjugated to streptavidin was added to enumerate IFN-γ–positive spots.

Proliferation assay

CellTrace Violet (5 μM) was used to stain wild-type B6 T cells, which were mixed with anti-CD3/CD28 mouse T cell activator Dynabeads (Life Technologies) at a T cell/bead ratio of 2:1. MDSCs were flow-sorted as granulocytic ($CD11b^+Ly6G^{hi}Ly6C^{lo}$) or monocytic ($CD11b^+Ly6G^-Ly6C^{hi}$) subtype from spleens of tumor-bearing mice and titrated into wells containing T cells plus beads. Cells were incubated in custom RPMI 1640 containing physiologic levels of L-arginine (150 μM) supplemented with 10% fetal calf serum, 50 μM 2-mercaptoethanol, 10 mM *N*-2-hydroxyethylpiperazine-*N*′−2-ethane sulfonic acid buffer, 1 mM sodium pyruvate, and penicillin/streptomycin (100 U/ml). To inhibit arginase activity, nor-NOHA was resuspended at 5 mg/ml in dimethyl sulfoxide and diluted to reach a final concentration of 300 μM. For NOS inhibition, L-NMMA was used at a concentration of 300 μM. Percent suppression was calculated as {[1 − (proliferation with MDSC/proliferation without MDSC)] × 100} for each respective group.

RT-PCR, quantitative PCR, and ELISA

Expression analysis of RNA was performed with RNueous-4PCR Kit (Life Technologies). Complementary DNA was synthesized using SuperScript III reverse transcriptase (Life Technologies). RT-PCR was performed with specific primers for murine arginase-1, iNOS, UTY, HPRT, and actin and amplified for 35 cycles. Quantitative RT-PCR TaqMan primers and probe specific for arginase-1, iNOS, and glyceraldehyde-3-phoshpate dehydrogenase were obtained through Applied Bio-systems and used according to the manufacturer's protocol. Human CXCL1 and CXCL8 levels and mouse CXCL1 and CXCL2 levels were performed on serum samples and cell culture supernatants as described in the manufacturer's protocol (R&D Systems). Normal ranges for human CXCL1 and CXCL8 were defined as the range of values spanning the means ± 2 SDs obtained from the study of serum from 21 healthy donors.

Patient samples

Metastatic/recurrent sarcoma and normal patient serum samples were obtained at the time of enrollment on Institutional Review Board–approved clinical trials of various

immunotherapies at the NCI, following informed consent. Histologies included osteosarcoma ($n = 6$), RMS ($n = 14$), Ewing sarcoma ($n = 20$), desmoplastic small round cell tumor ($n = 8$), synovial sarcoma ($n = 3$), and undifferentiated sarcoma ($n = 1$). The median age was 18 years (range, 5 to 34 years). Serum samples from healthy donors were obtained after informed consent and enrollment on National Institutes of Health Institutional Review Board–approved protocols.

Statistical analysis

Journal-formatted graphs were generated using GraphPad Prism software. Graphs represent mean values ± SEM. P values were calculated in each respective figure using Student's t test for comparing like groups or log-rank statistics for survival analyses. $P < 0.05$ was considered statistically significant and is illustrated with an asterisk (*).

Supplementary Material

Refer to Web version on PubMed Central for supplementary material.

Acknowledgments:

We thank T. Fry and M. Merchant (Pediatric Oncology Branch, NCI) for providing critical review of this manuscript and for providing patient samples, respectively. The 76–9 cell line was a gift from B. Weigel (University of Minnesota).

Funding: This work was supported in part by the NIH Intramural Research Program as well as by funding from the Liddy Shriver Sarcoma Initiative.

REFERENCES AND NOTES

1. Greenwald RJ, Freeman GJ, Sharpe AH, The B7 family revisited. Annu. Rev. Immunol 23, 515–548 (2005). [PubMed: 15771580]
2. Freeman GJ, Long AJ, Iwai Y, Bourque K, Chernova T, Nishimura H, Fitz LJ, Malenkovich N, Okazaki T, Byrne MC, Horton HF, Fouser L, Carter L, Ling V, Bowman MR, Carreno BM, Collins M, Wood CR, Honjo T, Engagement of the PD-1 immunoinhibitory receptor by a novel B7 family member leads to negative regulation of lymphocyte activation. J. Exp. Med 192, 1027–1034 (2000). [PubMed: 11015443]
3. Keir ME, Liang SC, Guleria I, Latchman YE, Qipo A, Albacker LA, Koulmanda M, Freeman GJ, Sayegh MH, Sharpe AH, Tissue expression of PD-L1 mediates peripheral T cell tolerance. J. Exp. Med 203, 883–895 (2006). [PubMed: 16606670]
4. Nishimura H, Okazaki T, Tanaka Y, Nakatani K, Hara M, Matsumori A, Sasayama S, Mizoguchi A, Hiai H, Minato N, Honjo T, Autoimmune dilated cardiomyopathy in PD-1 receptor-deficient mice. Science 291, 319–322 (2001). [PubMed: 11209085]
5. Ishida Y, Agata Y, Shibahara K, Honjo T, Induced expression of PD-1, a novel member of the immunoglobulin gene superfamily, upon programmed cell death. EMBO J. 11, 3887–3895 (1992). [PubMed: 1396582]
6. Dong H, Strome SE, Salomao DR, Tamura H, Hirano F, Flies DB, Roche PC, Lu J, Zhu G, Tamada K, Lennon VA, Celis E, Chen L, Tumor-associated B7-H1 promotes T-cell apoptosis: A potential mechanism of immune evasion. Nat. Med 8, 793–800 (2002). [PubMed: 12091876]
7. Pardoll DM, The blockade of immune checkpoints in cancer immunotherapy. Nat. Rev. Cancer 12, 252–264 (2012). [PubMed: 22437870]
8. Iwai Y, Ishida M, Tanaka Y, Okazaki T, Honjo T, Minato N, Involvement of PD-L1 on tumor cells in the escape from host immune system and tumor immunotherapy by PD-L1 blockade. Proc. Natl. Acad. Sci. U.S.A 99, 12293–12297 (2002). [PubMed: 12218188]

9. Hamanishi J, Mandai M, Iwasaki M, Okazaki T, Tanaka Y, Yamaguchi K, Higuchi T, Yagi H, Takakura K, Minato N, Honjo T, Fujii S, Programmed cell death 1 ligand 1 and tumor-infiltrating $CD8^+$ T lymphocytes are prognostic factors of human ovarian cancer. Proc. Natl. Acad. Sci. U.S.A 104, 3360–3365 (2007). [PubMed: 17360651]
10. Thompson RH, Gillett MD, Cheville JC, Lohse CM, Dong H, Webster WS, Krejci KG, Lobo JR, Sengupta S, Chen L, Zincke H, Blute ML, Strome SE, Leibovich BC, Kwon ED, Costimulatory B7-H1 in renal cell carcinoma patients: Indicator of tumor aggressiveness and potential therapeutic target. Proc. Natl. Acad. Sci. U.S.A 101, 17174–17179 (2004). [PubMed: 15569934]
11. Topalian SL, Hodi FS, Brahmer JR, Gettinger SN, Smith DC, McDermott DF, Powderly JD, Carvajal RD, Sosman JA, Atkins MB, Leming PD, Spigel DR, Antonia SJ, Horn L, Drake CG, Pardoll DM, Chen L, Sharfman WH, Anders RA, Taube JM, McMiller TL, Xu H, Korman AJ, Jure-Kunkel M, Agrawal S, McDonald D, Kollia GD, Gupta A, Wigginton JM, Sznol M, Safety, activity, and immune correlates of anti–PD-1 antibody in cancer. N. Engl. J. Med 366, 2443–2454 (2012). [PubMed: 22658127]
12. Brahmer JR, Tykodi SS, Chow LQ, Hwu WJ, Topalian SL, Hwu P, Drake CG, Camacho LH, Kauh J, Odunsi K, Pitot HC, Hamid O, Bhatia S, Martins R, Eaton K, Chen S, Salay TM, Alaparthy S, Grosso JF, Korman AJ, Parker SM, Agrawal S, Goldberg SM, Pardoll DM, Gupta A, Wigginton JM, Safety and activity of anti–PD-L1 antibody in patients with advanced cancer. N. Engl. J. Med 366, 2455–2465 (2012). [PubMed: 22658128]
13. Gabrilovich DI, Ostrand-Rosenberg S, Bronte V, Coordinated regulation of myeloid cells by tumours. Nat. Rev. Immunol 12, 253–268 (2012). [PubMed: 22437938]
14. Lesokhin AM, Hohl TM, Kitano S, Cortez C, Hirschhorn-Cymerman D, Avogadri F, Rizzuto GA, Lazarus JJ, Pamer EG, Houghton AN, Merghoub T, Wolchok JD, Monocytic $CCR2^+$ myeloid-derived suppressor cells promote immune escape by limiting activated CD8 T-cell infiltration into the tumor microenvironment. Cancer Res. 72, 876–886 (2012). [PubMed: 22174368]
15. Meadors JL, Cui Y, Chen QR, Song YK, Khan J, Merlino G, Tsokos M, Orentas RJ, Mackall CL, Murine rhabdomyosarcoma is immunogenic and responsive to T-cell-based immunotherapy. Pediatr. Blood Cancer 57, 921–929 (2011). [PubMed: 21462302]
16. Weigel BJ, Rodeberg DA, Krieg AM, Blazar BR, CpG oligodeoxynucleotides potentiate the antitumor effects of chemotherapy or tumor resection in an orthotopic murine model of rhabdomyosarcoma. Clin. Cancer Res 9, 3105–3114 (2003). [PubMed: 12912962]
17. Youn JI, Nagaraj S, Collazo M, Gabrilovich DI, Subsets of myeloid-derived suppressor cells in tumor-bearing mice. J. Immunol 181, 5791–5802 (2008). [PubMed: 18832739]
18. Rodriguez PC, Zea AH, Culotta KS, Zabaleta J, Ochoa JB, Ochoa AC, Regulation of T cell receptor CD3ζ chain expression by L-arginine. J. Biol. Chem 277, 21123–21129 (2002). [PubMed: 11950832]
19. Reutershan J, CXCR2—The receptor to hit? Drug News Perspect. 19, 615–623 (2006). [PubMed: 17299604]
20. Hodi FS, O'Day SJ, McDermott DF, Weber RW, Sosman JA, Haanen JB, Gonzalez R, Robert C, Schadendorf D, Hassel JC, Akerley W, van den Eertwegh AJ, Lutzky J, Lorigan P, Vaubel JM, Linette GP, Hogg D, Ottensmeier CH, Lebbé C, Peschel C, Quirt I, Clark JI, Wolchok JD, Weber JS, Tian J, Yellin MJ, Nichol GM, Hoos A, Urba WJ, Improved survival with ipilimumab in patients with metastatic melanoma. N. Engl. J. Med 363, 711–723 (2010). [PubMed: 20525992]
21. Robert C, Thomas L, Bondarenko I, O'Day S, Webber J, Garbe C, Lebbe C, Baurain JF, Testori A, Grob JJ, Davidson N, Richards J, Maio M, Hauschild A, Miller WH Jr., P. Gascon, M. Lotem, K. Harmankaya, R. Ibrahim, S. Francis, T. T. Chen, R. Humphrey, A. Hoos, J. D. Wolchok, Ipilimumab plus dacarbazine for previously untreated metastatic melanoma. N. Engl. J. Med 364, 2517–2526 (2011). [PubMed: 21639810]
22. Wolchok JD, Kluger H, Callahan MK, Postow MA, Rizvi NA, Lesokhin AM, Segal NH, Ariyan CE, Gordon RA, Reed K, Burke MM, Caldwell A, Kronenberg SA, Agunwamba BU, Zhang X, Lowy I, Inzunza HD, Feely W, Horak CE, Hong Q, Korman AJ, Wigginton JM, Gupta A, Sznol M, Nivolumab plus ipilimumab in advanced melanoma. N. Engl. J. Med 369, 122–133 (2013). [PubMed: 23724867]

23. Rodriguez PC, Ernstoff MS, Hernandez C, Atkins M, Zabaleta J, Sierra R, Ochoa AC, Arginase I–producing myeloid-derived suppressor cells in renal cell carcinoma are a sub-population of activated granulocytes. Cancer Res. 69, 1553–1560 (2009). [PubMed: 19201693]
24. Serafini P, Borrello I, Bronte V, Myeloid suppressor cells in cancer: Recruitment, phenotype, properties, and mechanisms of immune suppression. Semin. Cancer Biol 16, 53–65 (2006). [PubMed: 16168663]
25. Movahedi K, Guilliams M, Van den Bossche J, Van den Bergh R, Gysemans C, Beschin A, De Baetselier P, Van Ginderachter JA, Identification of discrete tumor-induced myeloid-derived suppressor cell subpopulations with distinct T cell–suppressive activity. Blood 111, 4233–4244 (2008). [PubMed: 18272812]
26. Dolcetti L, Peranzoni E, Ugel S, Marigo I, Fernandez Gomez A, Mesa C, Geilich M, Winkels G, Traggiai E, Casati A, Grassi F, Bronte V, Hierarchy of immunosuppressive strength among myeloid-derived suppressor cell subsets is determined by GM-CSF. Eur. J. Immunol 40, 22–35 (2010). [PubMed: 19941314]
27. Nausch N, Galani IE, Schlecker E, Cerwenka A, Mononuclear myeloid-derived “suppressor” cells express RAE-1 and activate natural killer cells. Blood 112, 4080–4089 (2008). [PubMed: 18753637]
28. Maenhout SK, Van Lint S, Emeagi PU, Thielemans K, Aerts JL, Enhanced suppressive capacity of tumor-infiltrating myeloid-derived suppressor cells compared with their peripheral counterparts. Int. J. Cancer 134, 1077–1090 (2014). [PubMed: 23983191]
29. Molon B, Ugel S, Del Pozzo F, Soldani C, Zilio S, Avella D, De Palma A, Mauri P, Monegal A, Rescigno M, Savino B, Colombo P, Jonjic N, Pecanic S, Lazzarato L, Fruttero R, Gasco A, Bronte V, Viola A, Chemokine nitration prevents intratumoral infiltration of antigen-specific T cells. J. Exp. Med 208, 1949–1962 (2011). [PubMed: 21930770]
30. Rot A, von Andrian UH, Chemokines in innate and adaptive host defense: Basic chemokinese grammar for immune cells. Annu. Rev. Immunol 22, 891–928 (2004). [PubMed: 15032599]
31. Fan X, Patera AC, Pong-Kennedy A, Deno G, Gonsiorek W, Manfra DJ, Vassileva G, Zeng M, Jackson C, Sullivan L, Sharif-Rodriguez W, Opdenakker G, Van Damme J, Hedrick JA, Lundell D, Lira SA, Hipkin RW, Murine CXCR1 is a functional receptor for GCP-2/CXCL6 and interleukin-8/CXCL8. J. Biol. Chem 282, 11658–11666 (2007). [PubMed: 17197447]
32. Kapanadze T, Gamrekelashvili J, Ma C, Chan C, Zhao F, Hewitt S, Zender L, Kapoor V, Felsher DW, Manns MP, Korangy F, Greten TF, Regulation of accumulation and function of myeloid derived suppressor cells in different murine models of hepatocellular carcinoma. J. Hepatol 59, 1007–1013 (2013). [PubMed: 23796475]
33. Yang L, Huang J, Ren X, Gorska AE, Chytil A, Aakre M, Carbone DP, Matrisian LM, Richmond A, Lin PC, Moses HL, Abrogation of TGFb signaling in mammary carcinomas recruits Gr-1+CD11b+ myeloid cells that promote metastasis. Cancer Cell 13, 23–35 (2008). [PubMed: 18167337]
34. Katoh H, Wang D, Daikoku T, Sun H, Dey SK, Dubois RN, CXCR2-expressing myeloid-derived suppressor cells are essential to promote colitis-associated tumorigenesis. Cancer Cell 24, 631–644 (2013). [PubMed: 24229710]
35. Trellakis S, Bruderek K, Hütte J, Elian M, Hoffmann TK, Lang S, Brandau S, Granulocytic myeloid-derived suppressor cells are cryosensitive and their frequency does not correlate with serum concentrations of colony-stimulating factors in head and neck cancer. Innate Immun. 19, 328–336 (2013). [PubMed: 23160385]
36. Ochoa AC, Zea AH, Hernandez C, Rodriguez PC, Arginase, prostaglandins, and myeloid-derived suppressor cells in renal cell carcinoma. Clin. Cancer Res 13, 721s–726s (2007). [PubMed: 17255300]
37. Waugh DJ, Wilson C, The interleukin-8 pathway in cancer. Clin. Cancer Res 14, 6735–6741 (2008). [PubMed: 18980965]
38. Mizukami Y, Jo WS, Duerr EM, Gala M, Li J, Zhang X, Zimmer MA, Iliopoulos O, Zukerberg LR, Kohgo Y, Lynch MP, Rueda BR, Chung DC, Induction of interleukin-8 preserves the angiogenic response in HIF-1α–deficient colon cancer cells. Nat. Med 11, 992–997 (2005). [PubMed: 16127434]

39. Sparmann A, Bar-Sagi D, Ras-induced interleukin-8 expression plays a critical role in tumor growth and angiogenesis. Cancer Cell 6, 447–458 (2004). [PubMed: 15542429]
40. Jijon HB, Buret A, Hirota CL, Hollenberg MD, Beck PL, The EGF receptor and HER2 participate in TNF-α-dependent MAPK activation and IL-8 secretion in intestinal epithelial cells. Mediators Inflamm. 2012, 207398 (2012). [PubMed: 22988345]
41. Fernando RI, Castillo MD, Litzinger M, Hamilton DH, Palena C, IL-8 signaling plays a critical role in the epithelial–mesenchymal transition of human carcinoma cells. Cancer Res. 71, 5296–5306 (2011). [PubMed: 21653678]
42. Benoy IH, Salgado R, Van Dam P, Geboers K, Van Marck E, Scharpé S, Vermeulen PB, Dirix LY, Increased serum interleukin-8 in patients with early and metastatic breast cancer correlates with early dissemination and survival. Clin. Cancer Res 10, 7157–7162 (2004). [PubMed: 15534087]
43. Zhang H, Maric I, DiPrima MJ, Khan J, Orentas RJ, Kaplan RN, Mackall CL, Fibrocytes represent a novel MDSC subset circulating in patients with metastatic cancer. Blood 122, 1105–1113 (2013). [PubMed: 23757729]
44. Seung LP, Rowley DA, Dubey P, Schreiber H, Synergy between T-cell immunity and inhibition of paracrine stimulation causes tumor rejection. Proc. Natl. Acad. Sci. U.S.A 92, 6254–6258 (1995). [PubMed: 7603979]
45. Srivastava MK, Zhu L, Harris-White M, Kar U, Huang M, Johnson MF, Lee JM, Elashoff D, Strieter R, Dubinett S, Sharma S, Myeloid suppressor cell depletion augments antitumor activity in lung cancer. PLOS One 7, e40677 (2012). [PubMed: 22815789]
46. Elias KM, Laurence A, Davidson TS, Stephens G, Kanno Y, Shevach EM, O'Shea JJ, Retinoic acid inhibits Th17 polarization and enhances FoxP3 expression through a Stat-3/Stat-5 independent signaling pathway. Blood 111, 1013–1020 (2008). [PubMed: 17951529]
47. Freeman BD, Danner RL, Banks SM, Natanson C, Safeguarding patients in clinical trials with high mortality rates. Am. J. Respir. Crit. Care Med 164, 190–192 (2001). [PubMed: 11463585]
48. Terabe M, Shimizu M, Mabuchi A, Matui S, Morikawa H, Kaneda K, Kakiuchi T, Yokomuro K, Unresponsiveness of intrahepatic lymphocytes to bacterial superantigen: Rapid development of suppressive Mac-1^{high} cells in the mouse liver. Hepatology 32, 507–513 (2000). [PubMed: 10960442]

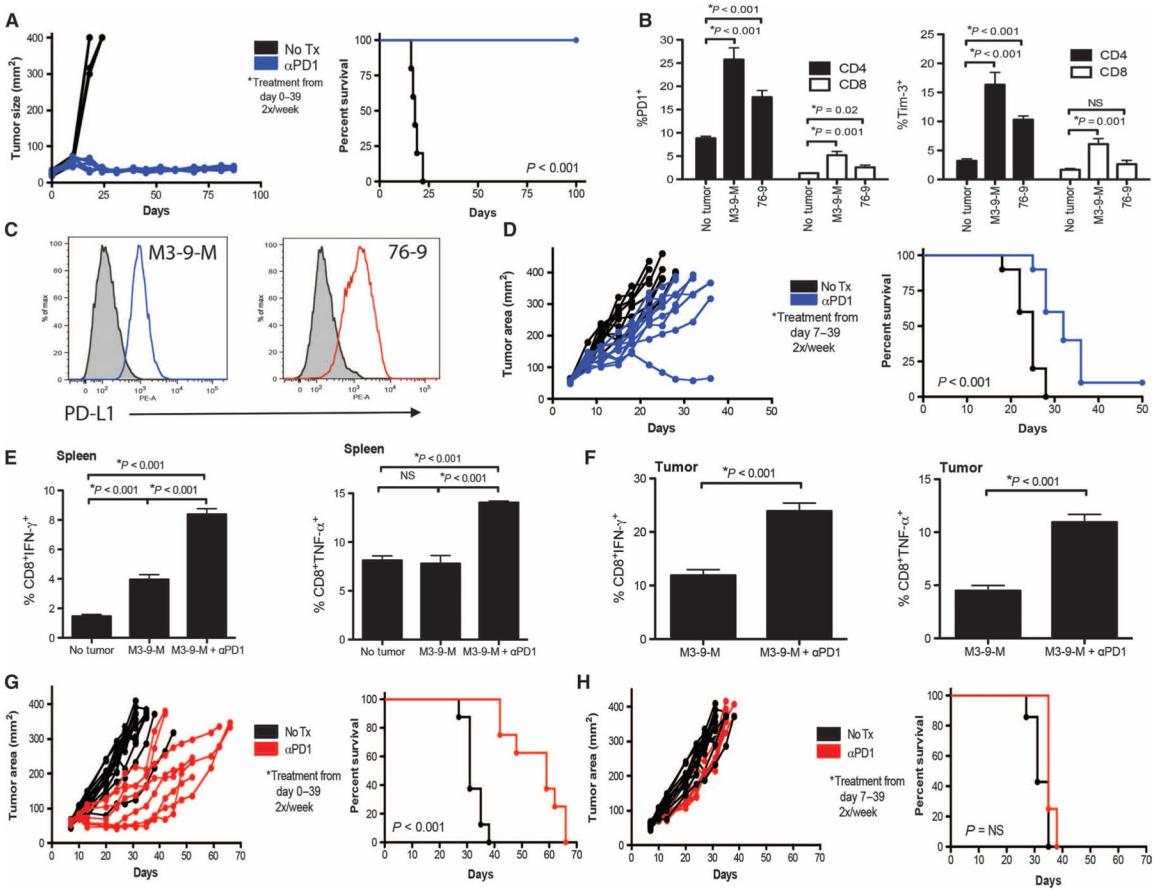

Fig. 1. Murine RMS is sensitive to anti-PD1 therapy.

Mice were orthotopically inoculated with M3-9-M RMS and control immunoglobulin G (No Tx), or anti-PD1 was administered intraperitoneally (200 μg per animal). (**A** and **D**) Survival and tumor size were monitored starting on day 0 (A) or on day 7 (D) and continued twice weekly until day 39. (**B**) Mice were inoculated with M3-9-M as above, and PD1 and Tim-3 expression on CD4 and CD8 T cells on day 20 is shown. NS, not significant. (**C**) Fluorescence-activated cell sorting (FACS) histograms showing surface expression of PD-L1 on M3-9-M and 76–9 RMS cells. (**E** and **F**) T cells from the spleen (E) and tumor (F) of mice from (A) were analyzed on day 12 for $CD8^+$ T cell production of intracellular IFN-γ and TNF-α after stimulation using soluble anti-CD3/anti-CD28. (**G** and **H**) Mice were inoculated with 76–9 RMS and treated as in (A) and (D). Experiments consist of five mice per group and are representative of at least three separate experiments. Two-tailed unpaired *t* test or Kaplan-Meier survival analysis was used to calculate *P* values.

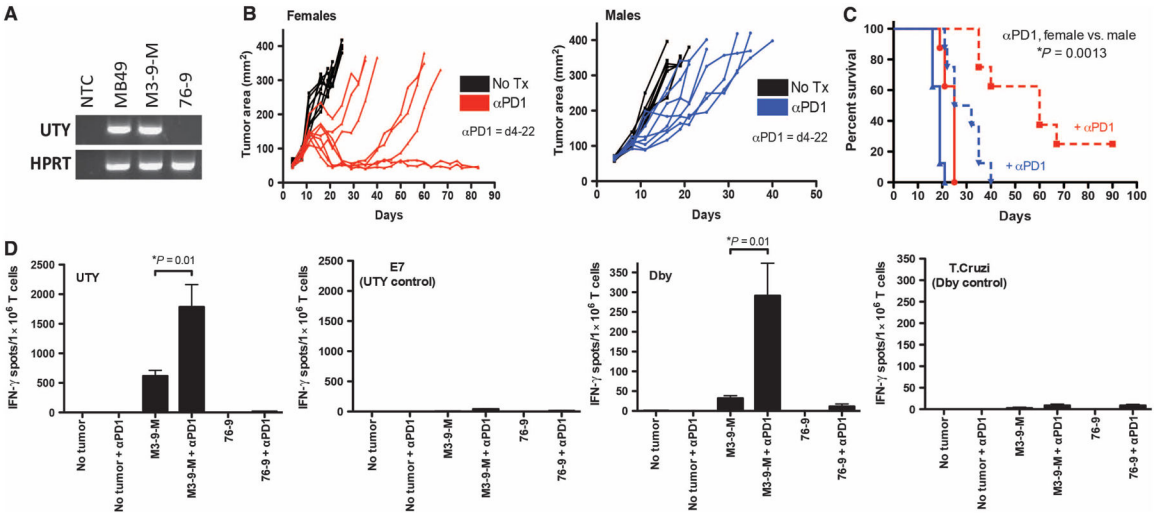

Fig. 2. Treatment with anti-PD1 augments T cell reactivity to HY antigens expressed by M3-9-M.

(**A**) Reverse transcription polymerase chain reaction (RT-PCR) of male-specific UTY on M3-9-M and 76–9 RMS cell lines. NTC, no template control; MB49, a known HY-expressing cell line used as a positive control; HPRT, used as an endogenous housekeeping control gene. (**B**) M3-9-M RMS cells (1×10^6) were injected into the gastrocnemius muscle of female (left) or male (right) wild-type (WT) B6 hosts, and cohorts were treated with anti-PD1 at 200 μg per animal from day 4 to day 22. Tumor growth curves of individual mice are shown. Kaplan-Meier survival curves (**C**) with log-rank statistics were used to compare the effects of anti-PD1 treatment in female (red) versus male (blue) hosts ($n = 8$ mice per group). (**D**) B6 female non-tumor-bearing mice or mice given M3-9-M or 76–9 tumor cells were treated with anti-PD1 starting at day 12. Splenocytes were harvested on day 25 and then stimulated with designated peptides overnight. IFN-γ–producing cells were enumerated using enzyme-linked immunospot (ELISpot). Five mice were used per group, and results shown are representative of two experiments. Two-tailed unpaired *t* test or Kaplan-Meier survival analysis was used to calculate *P* values.

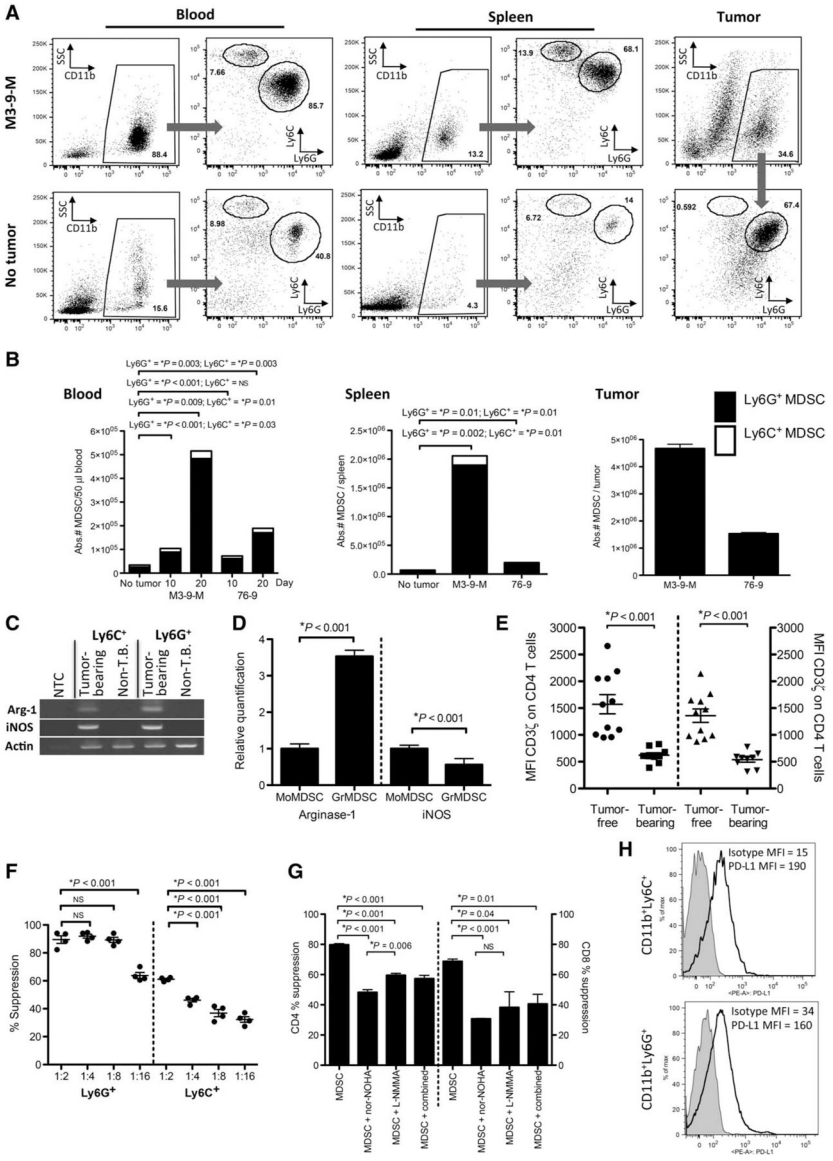

Fig. 3. Murine embryonal RMS predominantly expands GrMDSCs.

(**A** and **B**) Representative FACS plots (A) and absolute numbers (B) of MDSCs from blood on the days designated, and spleen and tumor ($n = 5$ per group) on day 20 after M3-9-M tumor inoculation. (**C**) RT-PCRwas performed to evaluate expression of arginase-1, iNOS in sorted populations of $CD11b^{+}Ly6G^{hi}$, and $CD11b^{+}Ly6C^{hi}$ from the spleens of tumor-bearing mice versus BM of non-tumor-bearing mice. NTC, no template control. (**D**) Relative quantification of arginase-1 and iNOS transcripts in $CD11b^{+}Ly6G^{hi}$ and $CD11b^{+}Ly6C^{hi}$ subsets sorted from tumor-bearing mice. (**E**) Peripheral blood was collected from non-tumor-bearing and M3-9-M-bearing mice, and intracellular CD3ζ mean fluorescent intensity (MFI) was plotted for $CD4^{+}$ and $CD8^{+}$ T cells. (**F**) $CD11b^{+}Ly6G^{hi}$ and $CD11b^{+}Ly6C^{hi}$ subsets were purified from the spleens of tumor-bearing mice and placed in a proliferation assay with purified CellTrace Violet-stained B6 T cells at the designated MDSC/T cell ratios. Anti-CD3/CD28 beads were used at a 1:2 ratio with T cells to induce proliferation.

Cells were harvested on day 5 and analyzed by FACS for Violet dilution. (**G**) CD11b $^{+}$Ly6G^{hi} cells were purified and placed in a proliferation assay as in (F) with the addition of nor-NOHA (arginase inhibitor) and L-NMMA (iNOS inhibitor), each at 300 μM. (**H**) PD-L1 expression on gated populations of MoMDSCs (top) and GrMDSCs (bottom). Data are representative of at least two independent experiments. Two-tailed unpaired *t* test was used to calculate *P* values.

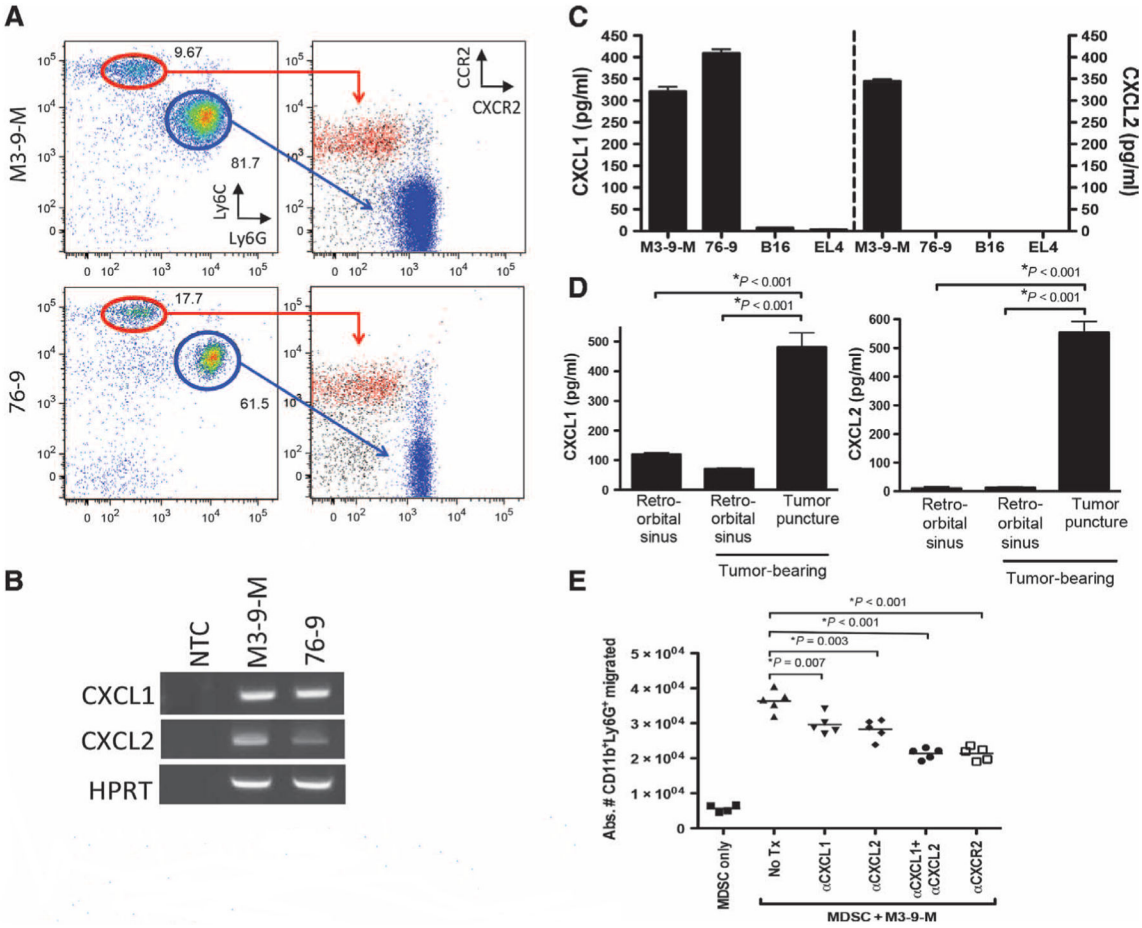

Fig. 4. Tumor-induced CD11b^{+}Ly6G^{hi} cells express CXCR2, and murine RMS produces CXCR2 ligands.

(**A**) Mice bearing M3-9-M or 76–9 tumors were analyzed for surface expression of CXCR2 and CCR2 on CD11b^{+}Ly6G^{hi} and CD11b^{+}Ly6C^{hi} subsets. (**B**) RT-PCR was performed to assess expression of CXCL1 and CXCL2 in M3-9-M and 76–9. NTC, no template control; HPRT, housekeeping control. (**C**) Protein analysis [enzyme-linked immunosorbent assay (ELISA)] of cell culture supernatants for CXCL1 and CXCL2. (**D**) ELISA analysis for CXCL1 (left panel) and CXCL2 (right panel) of serum obtained from blood samples taken from retro-orbital sinus of non–tumor-bearing and M3-9-M–bearing mice versus blood obtained directly from M3-9-M tumor puncture. (**E**) Peripheral blood CD11b^{+}Ly6G^{hi} cells were electronically sorted from mice bearing M3-9-M tumors placed in the top chamber of a Transwell. M3-9-M was plated in the bottom chamber, and the absolute number of MDSCs migrating from the top to the bottom chamber after 8 hours was enumerated. Blocking antibodies for CXCL1/CXCL2 and CXCR2 (4 μg/ml) were added at the beginning of the experiment. Two-tailed unpaired *t* test was used to calculate *P* values.

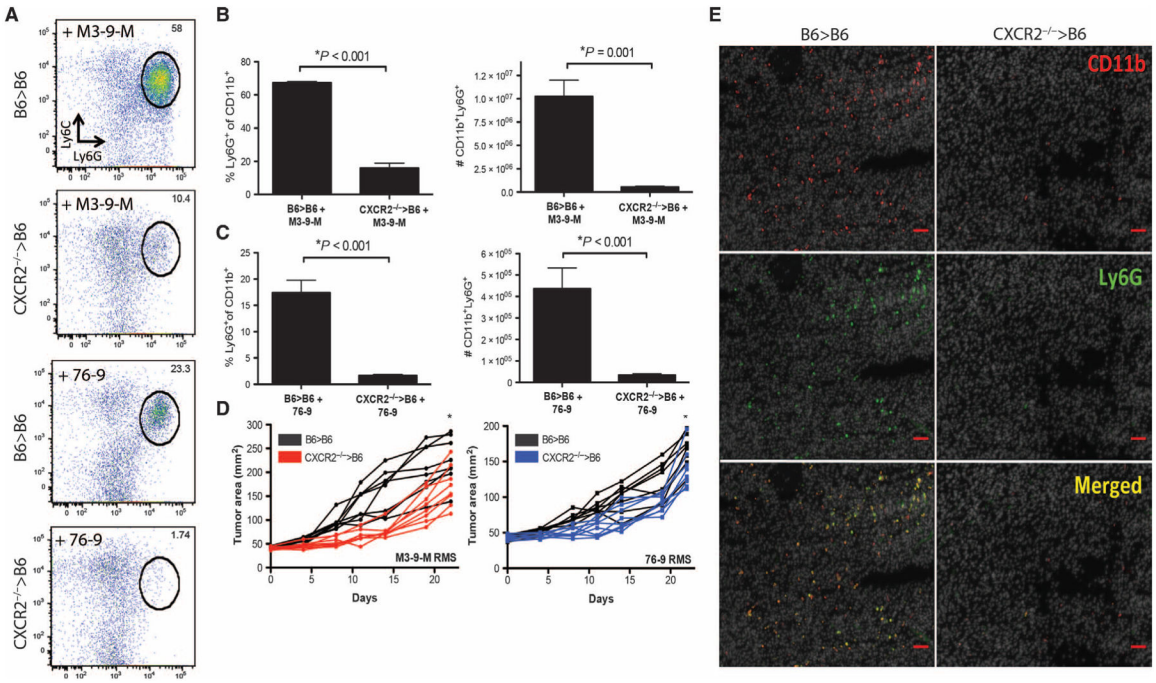

Fig. 5. CXCR2 is required for Ly6G^{hi} MDSCs homing to the tumor.

(**A**) WT B6 hosts were lethally irradiated and given syngeneic BM or CXCR2$^{-/-}$ BM as described in Materials and Methods. Animals were inoculated orthotopically with 1 × 10^6 M3-9-M (top) or 76–9 (bottom) on day 0. Tumors were harvested on day 22, and representative FACS plots gated on CD11b$^+$ cells are shown. (**B** and **C**) Percentage and absolute numbers of designated subsets in M3-9-M (B) or 76–9 (C) tumors on day 22. (**D**) Tumor growth curves for M3-9-M and 76–9 in mice with WT BM or CXCR2$^{-/-}$ BM. *P* values represent significance between the two groups at day 22. (**E**) Tissue sections of M3-9-M RMS from mice with WT or CXCR2$^{-/-}$ marrow stained with fluorescently conjugated CD11b (top), Ly6G (middle), or merged images (bottom). All panels costained with 4′,6-diamidino-2-phenylindole (gray). Scale bars, 50 μm. Experiments represent $n = 8$ mice per group. Two-tailed unpaired *t* test was used to calculate *P* values.

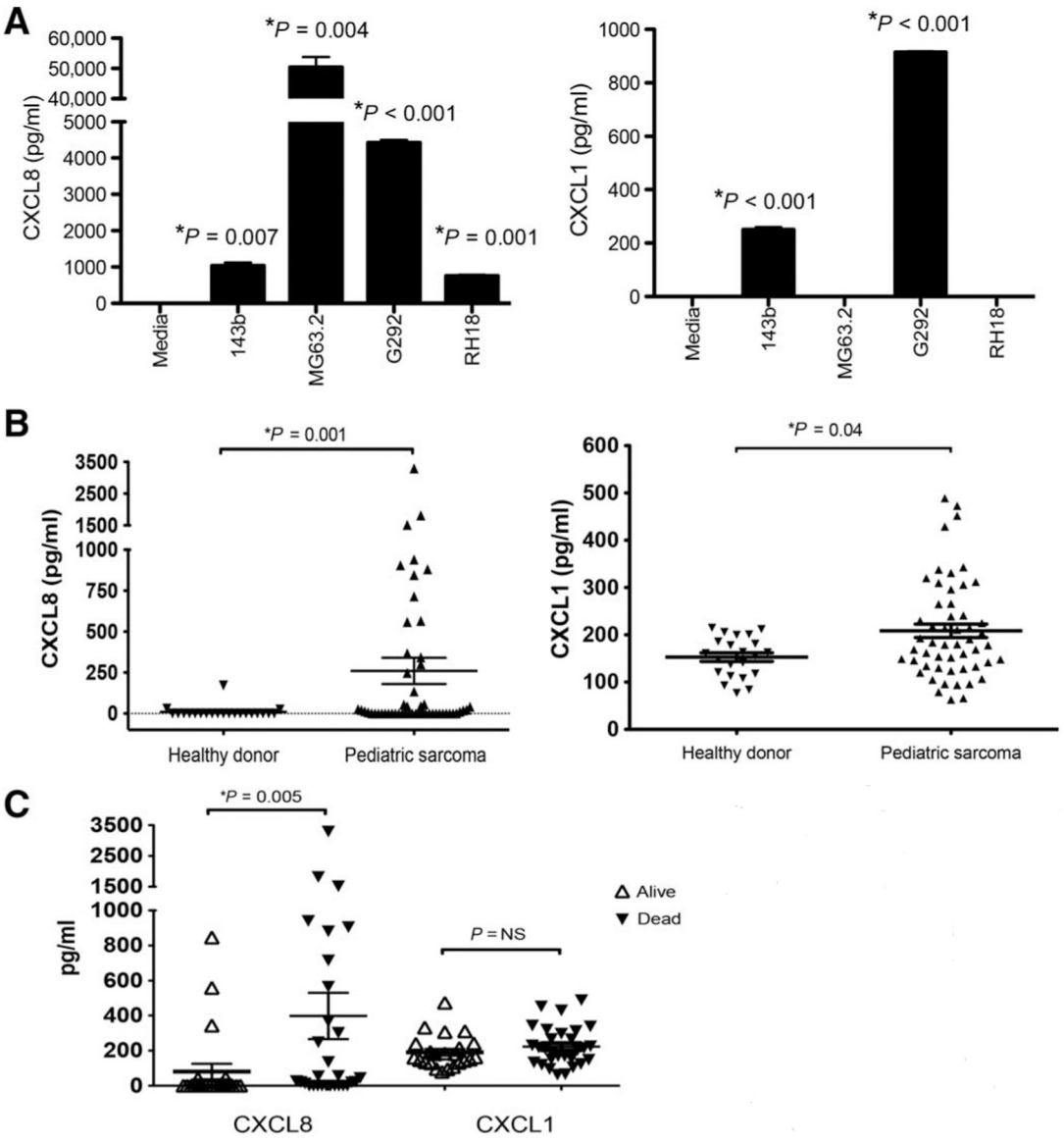

Fig. 6. Pediatric sarcoma tumors secrete CXCL1/CXCL8, and serumCXCL8 levels negatively correlate with survival in patients with pediatric sarcoma.

(**A**) CXCL8 and CXCL1 were measured in supernatant taken from in vitro–cultured human osteosarcoma (143b, MG63.2, and G292) and RMS (RH18) using ELISA. (**B**) CXCL1 and CXCL8 were measured by ELISA in serum samples collected from healthy donors ($n = 22$) and patients ($n = 53$) with pediatric sarcoma. (**C**) Serum CXCL8 is significantly higher in patients who died after enrollment on immunotherapy trials at NCI. Two-tailed unpaired t test was used to calculate P values.

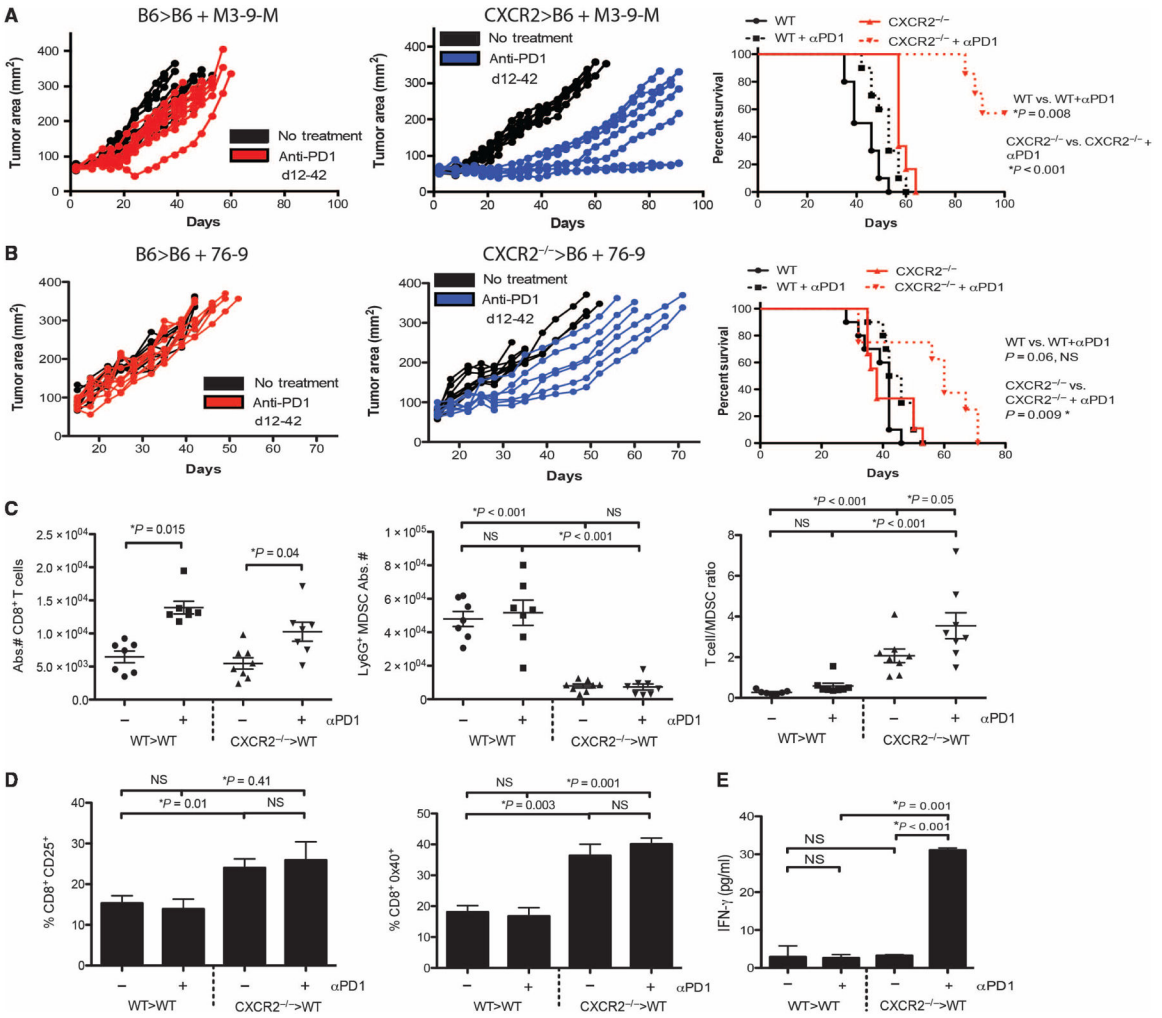

Fig. 7. PD1 checkpoint blockade is more effective in tumor-bearing hosts with CXCR2-deficient myeloid cells.

(**A** and **B**) Mice were inoculated with M3-9-M (A) or 76–9 (B) on day 0. Tumor growth in animals previously reconstituted with WT BM (left panel) or CXCR2$^{-/-}$ BM (middle panel) as described in Materials and Methods, and treated with control mAb or anti-PD1 as noted in the legend. Kaplan-Meier survival curves are shown in the right panel and were evaluated using log-rank statistics. (**C** and **D**) Cohorts of mice with M3-9-M RMS tumors were analyzed for absolute number of tumor-infiltrating T cells and Ly6G^{+} MDSCs, and CD25 and OX40 expression on tumor-infiltrating CD8^{+} cells 48 hours after initiation of anti-PD1 therapy (WT hosts, $n = 10$ per group; CXCR2$^{-/-}$ hosts, $n = 7$ per group). The ratio of T cell/MDSC was calculated. (**E**) Serum samples from cohorts of mice were analyzed for protein IFN-γ concentrations using ELISA. Two-tailed unpaired *t* test or Kaplan-Meier survival analysis was used to calculate *P* values.

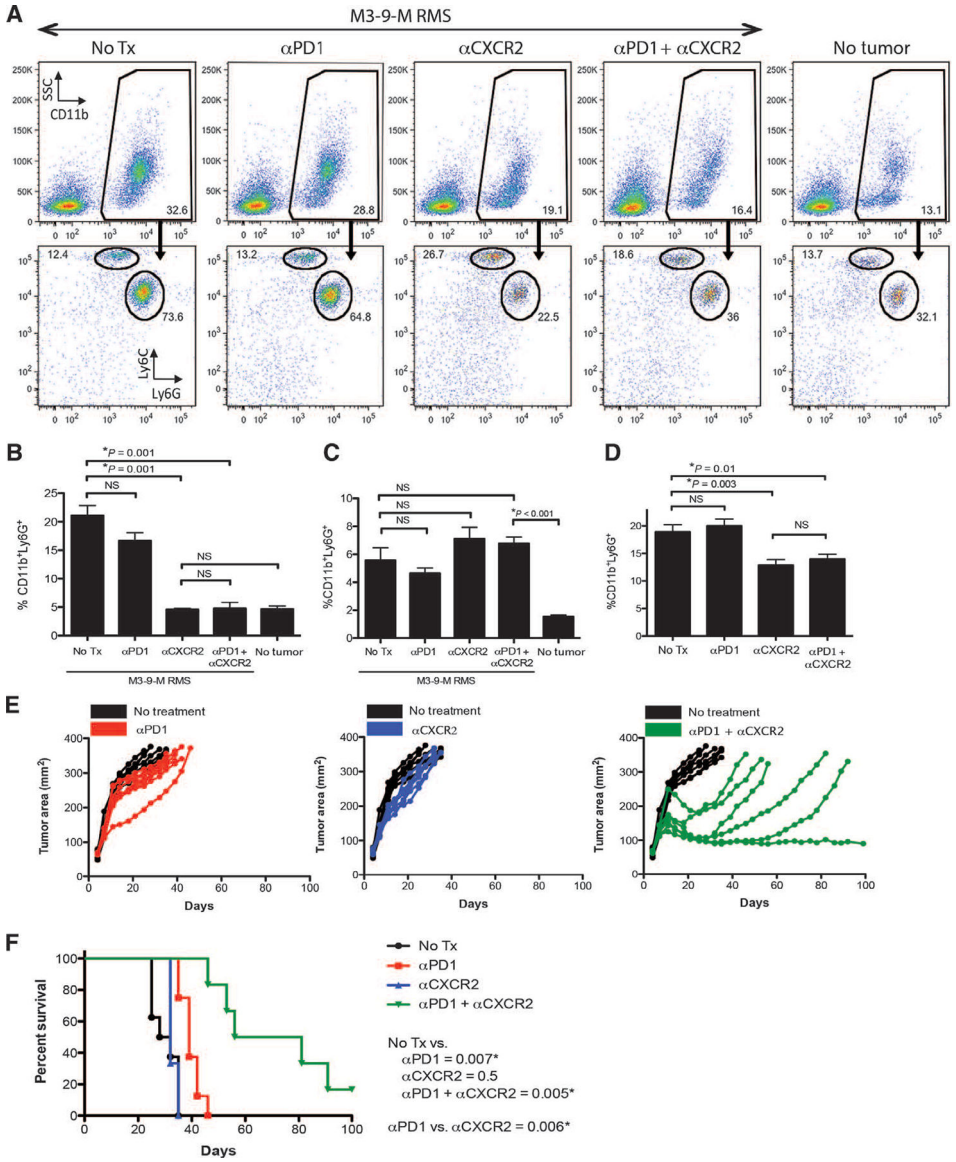

Fig. 8. The effectiveness of PD1 checkpoint blockade on established tumors is enhanced by anti-CXCR2 mAb therapy.

Mice were inoculated with M3-9-M RMS on day 0 as previously described. Cohorts were untreated and treated with anti-PD1 (200 μg per animal twice weekly starting on day 7 until day 35), anti-CXCR2 (200 μg per animal, days 6 and 10), or anti-CXCR2 plus anti-PD1. (**A** and **B**) Representative FACS plots (A) and cumulative data (B) from peripheral blood samples taken on day 15 from each group. (**C** and **D**) In a separate experiment, spleens (C) and RMS tumors (D) taken from untreated and treated mice were harvested and analyzed for MDSC infiltration. (**E** and **F**) Tumor growth curves and Kaplan-Meier survival curves for individual mice in (A). No Tx and anti-PD1 groups: $n = 8$ per group; anti-CXCR2 and anti-PD1 + anti-CXCR2 groups: $n = 6$ per group. Two-tailed unpaired t test or Kaplan-Meier survival analysis was used to calculate P values.